Space-and ground-based measurements of sulphur dioxide emissions from Turrialba Volcano (Costa Rica)

Article *in* Bulletin of Volcanology · June 2012

DOI: 10.1007/s00445-012-0631-z

CITATIONS
50

READS
289

9 authors, including:

Robin Campion
Universidad Nacional Autónoma de México
33 PUBLICATIONS **462** CITATIONS
SEE PROFILE

Maria Martinez Cruz
National University of Costa Rica
102 PUBLICATIONS **496** CITATIONS
SEE PROFILE

Thomas Lecocq
Royal Observatory of Belgium
90 PUBLICATIONS **649** CITATIONS
SEE PROFILE

Corentin Caudron
ISTerre
45 PUBLICATIONS **726** CITATIONS
SEE PROFILE

Bull Volcanol (2012) 74:1757–1770
DOI 10.1007/s00445-012-0631-z

RESEARCH ARTICLE

Space- and ground-based measurements of sulphur dioxide emissions from Turrialba Volcano (Costa Rica)

Robin Campion · Maria Martinez-Cruz · Thomas Lecocq · Corentin Caudron · Javier Pacheco · Gaia Pinardi · Christian Hermans · Simon Carn · Alain Bernard

Received: 27 April 2012 / Accepted: 9 June 2012 / Published online: 21 June 2012

Abstract Remotely sensed measurements of sulphur dioxide (SO_2) emitted by Turrialba Volcano (Costa Rica) are reported for the period September 2009–January 2011. These measurements were obtained using images from Advanced Spaceborne Thermal Emission and Reflexion radiometer, Ozone Monitoring Instrument and a ground-based UV camera. These three very different instruments provide flux measurements in good agreement with each other, which demonstrate that they can be integrated for monitoring SO_2 fluxes. Fluxes from Turrialba increased fourfold in January 2010, following a phreatic explosion that formed a degassing vent in the W crater of Turrialba. Since then, the SO_2 flux has remained high (30–50 kg/s) but seems to be showing a slowly decreasing trend. We interpret this evolution as the start of open vent degassing from a recently intruded magma body. The opening of the degassing vent decreased the confining pressure of the magma body and allowed the gases to bypass the hydrothermal system.

Keywords Remote sensing · SO_2 · Turrialba · OMI · ASTER · UV camera

Editorial responsibility: S. Calvari

Electronic supplementary material The online version of this article (doi:10.1007/s00445-012-0631-z) contains supplementary material, which is available to authorized users.

R. Campion (✉) · A. Bernard
Département des Sciences de la Terre et de l'Environnement,
Université Libre de Bruxelles,
50 Av. Roosevelt, CP160/02,
1050 Brussels, Belgium
e-mail: Robin.Campion@ulb.ac.be

M. Martinez-Cruz · J. Pacheco
Observatorio Vulcanológico y Sismológico de Costa Rica,
2346-3000 Heredia, Costa Rica

T. Lecocq · C. Caudron
Observatoire Royal de Belgique, Section de Séismologie,
Avenue Circulaire 3,
1180 Brussels, Belgium

G. Pinardi · C. Hermans
Institut d'Aéronomie Spatiale de Belgique (IASB),
Avenue Circulaire 3,
1180 Brussels, Belgium

S. Carn
Department of Geological and Mining Engineering and Sciences,
Michigan Technological University,
1400 Townsend Drive,
Houghton, MI 49931, USA

Introduction

Turrialba volcano is a basaltic–andesitic stratovolcano in Costa Rica (Fig. 1a), located at the Easternmost end of the Cordillera Volcánica Central, a chain of active volcanoes that results from the subduction of the Cocos plate under the Caribbean plate (e.g. Carr et al. 2003). Turrialba summit rises at 3,340 m a.s.l. and is only 9 km distant from Irazú volcano (Fig. 1b), another major volcano of the country. A major eruption would pose a significant threat to the Central Valley, the most populated part of Costa Rica. San Jose, the capital city of the country, is located 35 km W of the summit, in the direction of the prevailing winds. The rocks forming the volcanic edifice range from basalts to dacites. Three NE aligned summit craters open inside a depression breached to the NE. Reagan et al. (2006) did not find any debris avalanche deposits associated with this structure and suggested that it was formed by erosion during a hiatus in volcanic activity between 50,000 and 8,000 years BP. The last eruptive period, in 1864–1866, produced phreatomagmatic explosive activity and small pyroclastic flows (Reagan et al. 2006).

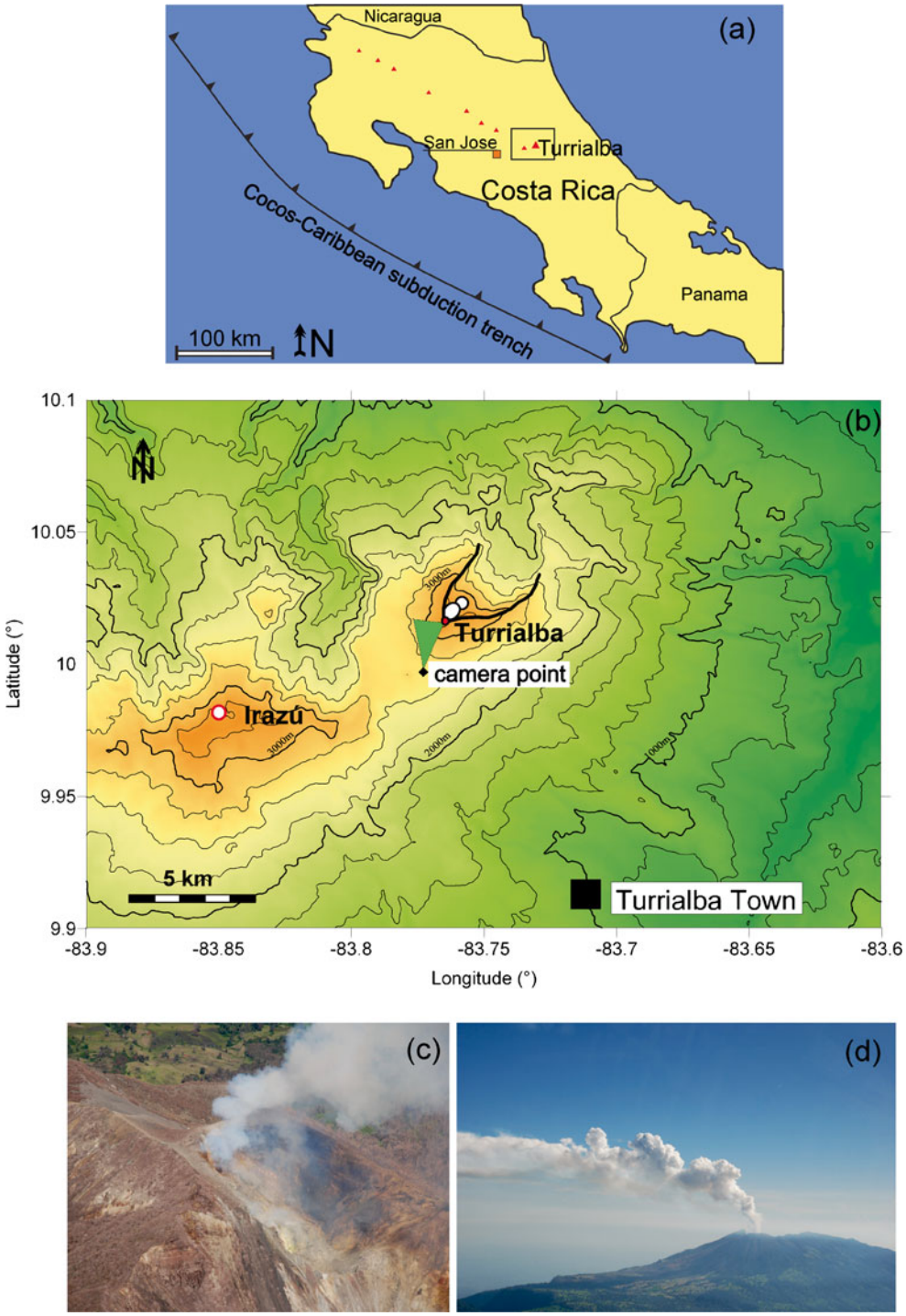

Fig. 1 **a** Map of Costa Rica showing the location of Turrialba Volcano. The *black rectangle* is enlarged in Fig. 1b. **b** Topographic map of the area of Turrialba volcano showing the active W crater (*red circle*) and the position from where UV camera measurements were done. **c** Degassing vent in the W crater on 29 May 2010. **d** Degassing plume seen from the W on 21 July 2010 (photos courtesy of Federico Chavarría-Kopper)

Fumarolic activity has shown a remarkable increase since 2002, with new fumarolic vents and fractures opening in- and outside of the crater area. Acidic gases and aerosol emissions have caused environmental acidification through wet and dry deposition. Severe chemical burns (chlorosis and necrosis) have affected the native mountain forest and the crops. Intense corrosion to the metallic parts of buildings and infrastructures was also reported (Fernández et al. 2010a, b, c). Due to prevailing winds, this damage was concentrated on the upper W half of the volcano. However, acidic deposition has recently been detected at localities as far as Santa Cruz de Turrialba, Pacayas, Llano Grande, the summits of Irazú and Barva volcanoes and Guápiles, which are as far as 30–40 km from the top of Turrialba volcano (Fernández et al. 2010c).

Vaselli et al. (2010) have reported the results of frequent gas analyses from the fumaroles in the central and W summit craters. Based on the increase in the SO_2/H_2S, (HCl+

HF)/CO_2 and S_{tot}/CO_2 ratios, they identified a three-stage evolution of the fumaroles:

1. During the hydrothermal stage, which characterised the fumarolic discharge since at least the 1980s until fall 2001 (e.g. Cheminée et al. 1983), the composition of the gas was dominated by H_2O, CO_2 and H_2S and their temperature was around 90 °C, the boiling point of water at the altitude of the volcano.
2. In the hydrothermal/magmatic stage, temperature was still low, but increasing concentrations of acidic gases (SO_2, HCl and HF) were found in the fumaroles. This was an indication that the hydrothermal system was still controlling the temperature of the fumarolic discharge, but was not able anymore to scrub all the acidic gases emitted at depth by the magma.
3. Finally, since 2007, both composition and high temperature (up to 400 °C) of the fumaroles indicate that the gases are directly supplied from the magma chamber with only limited interaction with the hydrothermal system.

To explain this complete evolution of the temperature and composition of the fumarolic discharge, Vaselli et al. (2010) proposed two different hypotheses:

1. A cyclical process in the mass and heat balance between the magma chamber and the hydrothermal system, as has already been inferred on other volcanoes such as Vulcano in Italy (Capasso et al. 1999), La Soufrière in Guadeloupe (Zlotnicki et al. 1992; Boichu et al. 2008), Galeras in Colombia (Fischer et al. 1996)
2. The intrusion of a magmatic body, which would supply increasing amounts of heat and acidic species until progressively drying out the overlying hydrothermal system and exceeding its scrubbing capacity (e.g. Symonds et al. 2001).

The implications of these two hypotheses for the future evolution of the volcano are profoundly different. While the first one implies only a localised risk of small-scale phreatic explosion, the second can lead to much stronger and potentially hazardous magmatic eruption or eruptive period. Vaselli et al. (2010) therefore recommended implementing a rigorous monitoring program to discriminate between these two hypotheses and forecast any potential magmatic activity. Based on the same geochemical data used by Vaselli et al. (2010), plus limited measurements of ground deformation and seismicity, Martini et al. (2010) concluded that the unrest was likely not caused by the intrusion of juvenile magma

SO_2 is one of the most important volcanic gases and arguably the easiest to measure by remote sensing. It is characteristically from high temperature gases and is thus a good indicator of the presence of magma at shallow depth. Therefore, measurements of SO_2 flux are widely recognised as a valuable parameter for volcano monitoring (e.g. review by Oppenheimer et al. 2011). Since the initial development of the COSPEC instrument in the seventies (e.g. Stoiber et al. 1983), tremendous technological advances have led to the deployment of permanent networks of miniaturised scanning UV spectrometers (e.g. Galle et al. 2009) and new instruments with imaging capacity at high spectral (Bobrowski et al. 2006) or temporal (SO_2 camera; e.g. Mori and Burton 2006) resolution. Remote sensing of SO_2 is also possible from satellites operating either in the ultraviolet or in the infrared. However, among the wealth of satellites capable of measuring SO_2 (e.g. review by Thomas and Watson 2010), only ASTER and OMI have the necessary combination of spectral and spatial resolution to detect and quantify low altitude emissions produced by passive volcanic degassing.

This paper presents SO_2 flux measurements obtained by processing images of OMI and ASTER satellites from September 2009 to January 2011 and with a UV camera in March 2010. We demonstrate the consistency and complementarity of the SO_2 flux data obtained from these three methods. We also discuss the insights that these measurements provide into the ongoing magmatic-hydrothermal processes under Turrialba Volcano. Only a few SO_2 flux measurements from Turrialba have been published prior to this study, in Martini et al. (2010). Those measurements, resulting from irregular mini-DOAS traverses, showed that flux values increased from 0 to ~10 kg/s between 2002 and 2008, in coincidence with the above-mentioned evolution of the fumaroles' chemistry.

Instruments and methods

The key characteristics of the three instruments used in this work are compared in Table 1. ASTER is an imaging multispectral radiometer that measures the thermal infrared radiation (TIR) emitted by the Earth's surface in five spectral bands numbered B10–B14 and respectively centred at 8.29, 8.63, 9.07, 10.66 and 11.32 μm. ASTER has a 90-m resolution in the thermal infrared, which allows measurements of SO_2 in small-scale plumes, such as those typically produced by passive degassing. Its sensitivity to SO_2 is lower than OMI because the SO_2 absorption cross section is three orders of magnitude smaller in the TIR than in the UV. However, the much finer ground resolution of ASTER compensates for its lower sensitivity, so that the detection limit in terms of lowest detectable flux is roughly equivalent between the two sensors (see Table 1). ASTER images are only 60 km wide and are not acquired in continuous mode (Pieri and Abrams 2004). Instead, image acquisitions can be programmed according to the needs of the users' community, so that the rate of image acquisitions can be quite variable, between twice a week and a few per year. ASTER images were processed with the radiance ratio algorithm (Campion et al. 2010) to retrieve SO_2 column amounts (CA). The main advantage of this algorithm is its low

Table 1 Summary of the characteristics of the instruments used in this study. The sensitivity is defined as the 1σ noise over an SO_2-free zone for a typical Turrialba scene. The detection limit is calculated as the flux measured over a profile of three pixels containing a column amount of 3σ, and with a 5 m/s wind

	ASTER	OMI	UV camera
Wavelength range	8–12 μm	300–330 nm	300–330 nm
Pixel dimension	90×90 m	13×24 km[a]	2×2 m[b]
Sensitivity (g/m^2)	1	8.5×10^{-3}	0.3
Detection Limit (kg/s)	4	5–10[c]	0.03
References	Campion et al. (2010)	Yang et al. (2007)	Mori and Burton (2006)
		Carn et al. (2008)	Kern et al. (2010b)

[a] Nadir size

[b] Pixel size for an observation distance of 2,800 m

[c] Depending on the direction of the plume

dependence on surface emissivity, water vapour and sulphate aerosols. This is especially useful in the tropical atmosphere, where atmospheric humidity is high and plumes usually contain a high load of condensed aerosol. The uncertainty on the retrieved CAs is usually about 20 % for Turrialba plumes. This value is calculated automatically in the algorithm by retrieving SO_2 with a 500-m biased altitude and taking into account the noise equivalent SO_2 over a region outside of the plume. Meteorological clouds located under the volcanic plume increase this uncertainty significantly, due to reduced thermal contrast, while clouds located between the plume and the sensor completely mask the SO_2 absorption. However, the band ratio algorithm contains a cloud detection routine excluding them from the analysis. Plume temperature, a very important parameter for the accuracy of the retrievals, is estimated using opaque portions of the plume, often encountered close to the vent. Traverses are traced perpendicularly to the plume, and the flux is computed by summing the CA along the traverses and multiplying by the wind speed. The wind speed value comes from the European Center for Medium-Range Weather Forecasts (ECMWF) model at the time of overpass, coordinates of the volcano and plume altitude.

OMI is an imaging spectrometer that measures the backscattered ultraviolet radiation (BUV) from the Earth's surface and atmosphere over a 2,700-km wide swath (Levelt et al. 2006). OMI pixels have cross- and along-track dimensions of respectively 24 and 13 km at nadir, the former increasing gradually towards the edges of the swath. This ground resolution is unprecedented for a BUV satellite and, together with its high sensitivity to SO_2 (~1.5×10^{-2} g/m^2), allows OMI to detect small-scale plumes produced by passive volcanic degassing (e.g., Carn et al. 2008). OMI SO_2 data are produced in near real time using two algorithms. The Band Residual Algorithm (Krotkov et al. 2006) was designed for achieving a high sensitivity to low abundance boundary layer SO_2, while the linear fit (Yang et al. 2007) is better suited for volcanogenic SO_2, which has usually a higher altitude and concentration. We used the standard SO_2 product from OMI, which is publicly available at http://mirador.gsfc.nasa.gov/cgi-bin/mirador/collectionlist.pl?keyword=omso2. Images were downloaded as HDF files containing four values of the SO_2 CA, retrieved using four different a priori vertical profiles. These are called PBL_SO2, TRL_SO2, TRM_SO2 and STL_SO2 and correspond to SO_2 plumes centred at 0.7, 2.5, 7.5 and 15 km, respectively. For this study, the effective SO_2 CA of each pixel is interpolated using these four values and an altitude of 3,500 m (for ECMWF wind speed of more than 6 m/s at the volcano elevation) or 4,000 m (for slower ECMWF wind value). This is based on visual observation of the plume and wind speed measurements registered throughout the year 2010 by OVSICORI. The accuracy of OMI measurements of SO_2 CA depends strongly on the estimated plume height. For the typical altitude of Turrialba plume, sensitivity tests show that a 500-m overestimation of the plume altitude yields a ~20 % underestimation in the retrieved CA. Further error (10–20 % according to Yang et al. 2007) arises from the non-linear absorption of UV radiations by high CAs of SO_2 and from the sub-pixel distribution of the meteorological clouds and the SO_2 plume. Fluxes are computed from the images using a routine written in Interactive Data Language (IDL). This routine defines transects as lines or columns of pixels across the plume, sums the CAs of every pixels of the profile and multiplies that sum by the wind speed times the cosine of the angle between the transect and the plume direction. This routine is an adaptation of the procedure that has been applied for performing COSPEC measurements on a mobile platform (e.g. Stoiber et al. 1983). The final flux value computed from an OMI image is obtained by averaging the fluxes from the first six profiles, excluding the one that is the closest to the volcano to avoid subpixel dilution.

Ground-based data were collected using an Apogee Alta U260 charge-coupled device camera equipped with two narrowband pass filters, centred at 310 and 330 nm, mounted on a manual filter switcher (Mori and Burton

2006). Images were acquired every 5 s with a diaphragm opened at F11 and an exposure time varying between 0.5 and 0.8 s, identical for both filters. All the images were corrected for vignetting using 25 images of the cloud free sky (Kantzas et al. 2010) acquired about 1 h before. For each pair of image, the normalised absorbance is calculated, on a pixel per pixel base with

$$A_{i,j} = \log\left(\frac{I^A_{i,j}}{I^B_{i,j}}\right) - \log\left(B_{i,j}\right) \quad (1)$$

$I^A_{i,j}$ and $I^B_{i,j}$ are the vignette corrected irradiances measured with filter A and B, respectively, and $B_{i,j}$ is the synthetic background absorbance, constructed with a planar extrapolation based on SO_2-free regions of the pair of images (Kantzas et al. 2010). The normalised absorbance image is then compared to calibration images of SO_2-free sky. These calibration images were acquired at the end of each series of 100 image pairs using quartz cells containing 0, 1,000, 1,500 and 2,000 ppm m of SO_2. Wind speed was calculated by measuring the displacement of SO_2 spikes and troughs measured over a profile parallel to wind direction. A similar method was developed independently by Tamburello et al. (2011). SO_2 flux is calculated by summing the SO_2 slant concentrations of each pixels of a profile perpendicular to the plume and multiplying by the equivalent length of the pixels and by the wind speed. All these operations are executed automatically using the program RobtraiteCamSO2, written in IDL (Campion, unpublished data, 2011).

Error on flux measurements comes from radiative transfer effects (Kern et al. 2010a, b), from error on the calibration cells concentrations, and from uncertainty on the observation geometry. The overall error on the flux is calculated with the standard error propagation formula (e.g. Stoiber et al. 1983).

$$\Delta F = \sqrt{(\Delta C_C)^2 + (\Delta C_R)^2 + (\Delta l)^2 + (\Delta v)^2} \quad (2)$$

ΔC_C is the error in the calibration of the instrument. Image of the calibration cells were acquired with the same exposure time and lens aperture as measurement images, following the recommendations of Dalton et al. (2009). Our calibration cells, home-built and measured in the lab with a high precision Fourier transform UV spectrometer, are accurate to 2 % and cover most of the range of concentrations encountered in the Turrialba plume. ΔC_R is the error due to radiative transfer effects. Kern et al. (2010a) have studied the two processes responsible for systematic error in SO_2 measurement using UV spectrometry. The first one, known as light dilution, leads to underestimating the CA and increases with the observation distance and the aerosol content of the atmosphere. The second effect, multiple scattering of light inside the plume, causes an overestimation the CA measurements, and increases with the content and scattering coefficient of the aerosol in the plume. Conditions were favourable during the 2 days of fieldwork, with a very clear atmosphere, an aerosol-poor plume, and a 2.8-km viewing distance. Therefore ΔC_R is estimated to 20 %. Δl is the error in the plume to instrument distance, a function of the plume direction. It is estimated to 10 %, as we drove beneath the plume to locate its centre before starting the measurements with the camera. Δv is the error on the wind velocity and is also estimated to 10 % (Mori and Burton 2006). The final calculation of the error on the flux measurements with the UV camera is thus calculated to ~25 %. For satellite measurements, the final error on fluxes is calculated with the same error propagation formula as Eq. 2, considering the error on the individual CA measurements, detailed earlier, and a 25 % error on the wind velocity.

Results

The SO_2 fluxes measured with the three techniques described above are reported in Table 2 and displayed graphically in Fig. 2. Average fluxes ranged from 5 to 52 kg/s, showing a dramatic increase in the beginning of 2010 and a slow gradual decrease afterwards.

During the reporting period, 48 TIR images of Turrialba volcano were acquired by ASTER. Many of them have too much cloud to providing useful information and were thus not analysed. A screening was also done before analysing OMI images, excluding the images where the SO_2 plume was partly masked by high altitude clouds and those where no clear plume transport direction could be identified. SO_2 maps produced with ASTER images are displayed in Fig. 3. ASTER's ground resolution is high enough for identifying the plume direction and structure and for interpreting its transport mode following the terminology proposed by Kinoshita (1996). Coherent plume transport (linear dispersion) predominates, except perhaps on 21 April, where a fan structure in a weak wind field could be inferred. These observations suggest that, on the considered days, volcano topography had little influence over the wind field at the plume altitude. The ASTER SO_2 maps show homogeneous plumes, with no obvious puffs.

Some of the OMI SO_2 maps analysed in this work are displayed in Fig. 4. The pixel size is much coarser than for ASTER, but the noise in the retrieval is two orders of magnitude lower. On many days of 2009, no plume could be detected by visual inspection of the SO_2 images. The detection limit of OMI in terms of flux depends on the reflectivity of the underlying surface, on the plume altitude and on the dispersion of the SO_2 by the local wind fields. In 2009, the SO_2 plume could be detected only in weak winds and low cloud conditions. In 2010, however, SO_2 is detected

Table 2 SO_2 dataset from Turrialba Volcano

Date (dd/mm/yy)	Flux	Estim.error (%)	Height (m)	Windspeed (m/s)	Method	DNSI (%)	DNOI (%)
9/09/2009	9	50	4,000	5	ASTER		
12/09/2009	8	40	4,000	3.5	OMI		
23/10/2009	bd	bd	3,500	6.5	OMI		
16/11/2009	5	40	3,500	7	OMI		
6/01/2010	58	40	4000	7.5	OMI	47	28
10/01/2010	31	40	3,500	11	OMI	−29	−35
15/01/2010	42	30	3,800	7	ASTER	7	5
17/01/2010	40	40	4,000	4.5	OMI	33	3
31/01/2010	39	30	3,800	8	ASTER	−33	31
31/01/2010	52	30	3,800	8	ASTER	25	48
16/02/2010	39	30	3,400	8	ASTER	−23	31
27/02/2010	27	40	4,000	3.5	OMI	−63	−78
7/03/2010	44	40	4,000	4	OMI	−9	25
15/03/2010	48	40	3,500	10	OMI	31	0
15/03/2010	30	25	3,600	8	UV cam	−17	−60
16/03/2010	35	25	3,600	10	UV cam		6
21/04/2010	48	50	4,500	5	ASTER	27	31
23/04/2010	33	40	3,500	13	OMI	27	−6
18/05/2010	24	40	4,000	5	OMI	−46	−46
12/06/2010	22	40	4,000	4	OMI	46	−59
24/06/2010	35	30	4,000	6	ASTER	31	46
06/08/2010	35	40	4,000	4.5	OMI	37	0
12/09/2010	24	30	3,500	8	ASTER	−17	21
11/10/2010	19	40	4,000	4.5	OMI		−47
18/01/2011	18	40	3,500	5	ASTER		

These data are also presented graphically in Fig. 2

bd SO_2 was below detection limit, *DNSI* relative difference between the considered flux value and the next value measured with the same instrument, *DNOI* relative difference between the considered flux value and the next value measured with another instrument (ASTER for values obtained with OMI, OMI for values obtained with ASTER and both satellites for UV camera measurements)

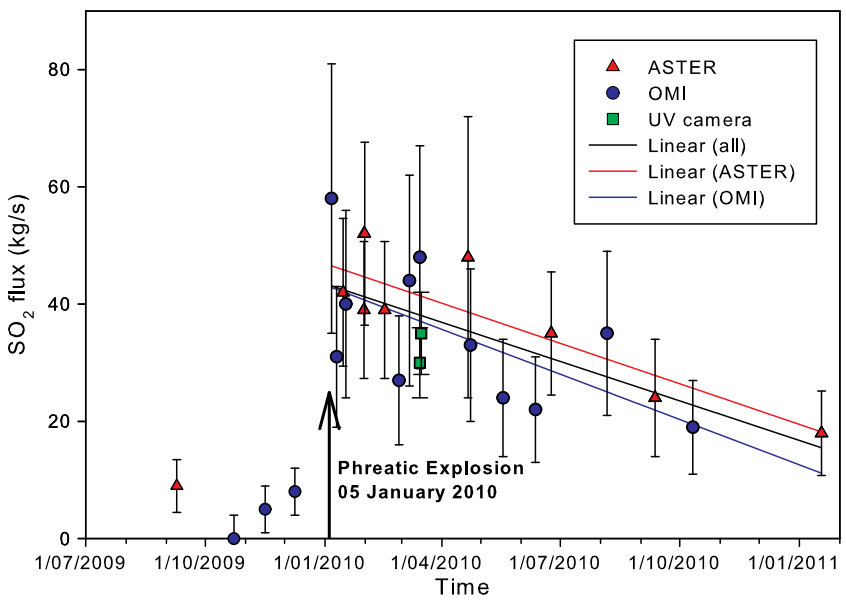

Fig. 2 Time evolution of the SO_2 fluxes emitted by Turrialba from September 2009 to January 2011. The *arrow* marks the onset of the phreatic eruption on 5 January 2010. Error bars are the same as in Table 2. The regression lines were obtained for the data obtained after 5 January 2010 with ASTER (*red*), OMI (*blue*) and all three instruments together (*black*)

on nearly every image, and the SO_2 maps show that emissions from Turrialba affect wide areas around the volcano.

Measurements with the UV camera were taken from a location 2.8 km S of the active crater (see map in Fig. 1), during a campaign on 15 and 16 March 2010. Examples of SO_2 images are shown in Fig. 5. More results are also available as GIF animations in the Supplementary material available in the online version of the article. The presence of concentrated puffs is obvious in the Fig. 5. This is also reflected in the periodic flux variation in Fig. 6, each peak in the graph being associated with a puff crossing the measurement line. Interestingly, the puffs were not detected on the satellite images, presumably because their typical size (100–200 m according to the UV camera measurements) is too small to be resolved by ASTER and a fortiori by OMI.

Discussion

Comparison between the three methods

Figure 2 shows that the fluxes measured using the three techniques follow a visually similar evolution and generally agree within each other's error bars. Despite the lack of simultaneity in image acquisition, a more quantitative comparison of the three techniques can be obtained using two approaches: the difference between pairs of successive images and the comparison of the regression lines associated to each technique. These two approaches are detailed below.

The two last columns of Table 2 help to assess the agreement of the three methods in a more quantitative way. In the seventh column, the DNSI is defined as the difference between the flux values obtained with two successive images from the same instrument. This parameter reflects both the natural variability of the flux and the uncertainty on the measurements technique. In the last column, the DNOI is defined as the difference between two successive flux values obtained with two different techniques and is proportional to the flux variability, the error on the techniques, plus the disagreement between the two techniques. These two parameters were not calculated for the four first entries of the dataset due to a marked change in the degassing behaviour in early January 2010 (see next section). The average of the absolute value of the DNSI for ASTER, OMI and the UV camera are 23, 34 and 17 %, respectively, which is close to the error estimated theoretically, even if the data set contains too few UV camera entries to be really significant. On the other hand, the average of the absolute values of the DNOI over the whole dataset is only 29 %, which is slightly inferior to the average DNSI over the whole dataset (31 %). This demonstrates that using the three techniques together does not produce a significantly higher variability than using only one of them.

Three linear regressions were applied to the flux measurements obtained after January 2010. The resulting trend lines are respectively $F=42.8–0.0833*T$ with $R^2=0.39$ for the OMI data, $F=46.5–0.0751*T$ with $R^2=0.75$ for the ASTER data and $F=43.1–0.731*T$ with $R^2=0.46$ for the whole dataset, F being the SO_2 flux and T the time elapsed since 5 January 2010, when the first elevated flux was measured. The R^2 of these trend lines is rather low because it reflects both error on measurements and small timescale variation of the actual SO_2 emission rate. These trend lines are displayed in Fig. 2. Numerically these three trend lines are quite close to each others. In the detail, OMI trend line appears to have a stronger spread and to be slightly lower both in its slope coefficient and in its y intercept, than those of ASTER and of the whole dataset. We believe that this might be an effect of OMI's coarser pixel size, although further investigations are required to ascertain this. The two UV camera data appear to fall slightly below all three trend lines, with residuals of −8 and −3 kg/s. Although they are too few measurement points to be really significant, this could reflect some systematic underestimation by the UV camera due to light dilution (Mori et al. 2006, Kern et al. 2010a). Again more research is needed to clarify this.

Agreement between the three techniques is overall very good despite these minor discrepancies, which suggests that their results can be integrated for monitoring purposes. This is an important conclusion of this study because each of these methods is complementary with the two others. OMI provides frequent images that can be exploited even if there is a low cloud layer between the surface and the plume (a case that precludes the use of the UV camera and reduces the precision of ASTER). However, the precision of flux measurements is limited due to the coarse pixel size of the instrument. ASTER has better imaging capacity and precision, except for cloudy scenes, but its scarce and irregular coverage can represent an issue for continuous monitoring. It is also worthwhile noting that both satellite methods yield flux values that depend on auxiliary data (plume height and wind speed) that can themselves be inaccurate. With the UV camera, on the contrary, these parameters can easily be determined. Furthermore, the high temporal and spatial resolution of the UV camera allows insights into the short timescale variation in magma degassing that the satellites cannot access. Obtaining accurate measurement with a UV camera, however, requires suitable observation conditions and the deployment of a two-person team in the field, whereas satellite measurements can be made comfortably from an office.

Temporal evolution and significance of the SO_2 fluxes

The SO_2 fluxes values measured at Turrialba since early January 2010 have been remarkably high, although no magma has been emitted so far. They place Turrialba among the

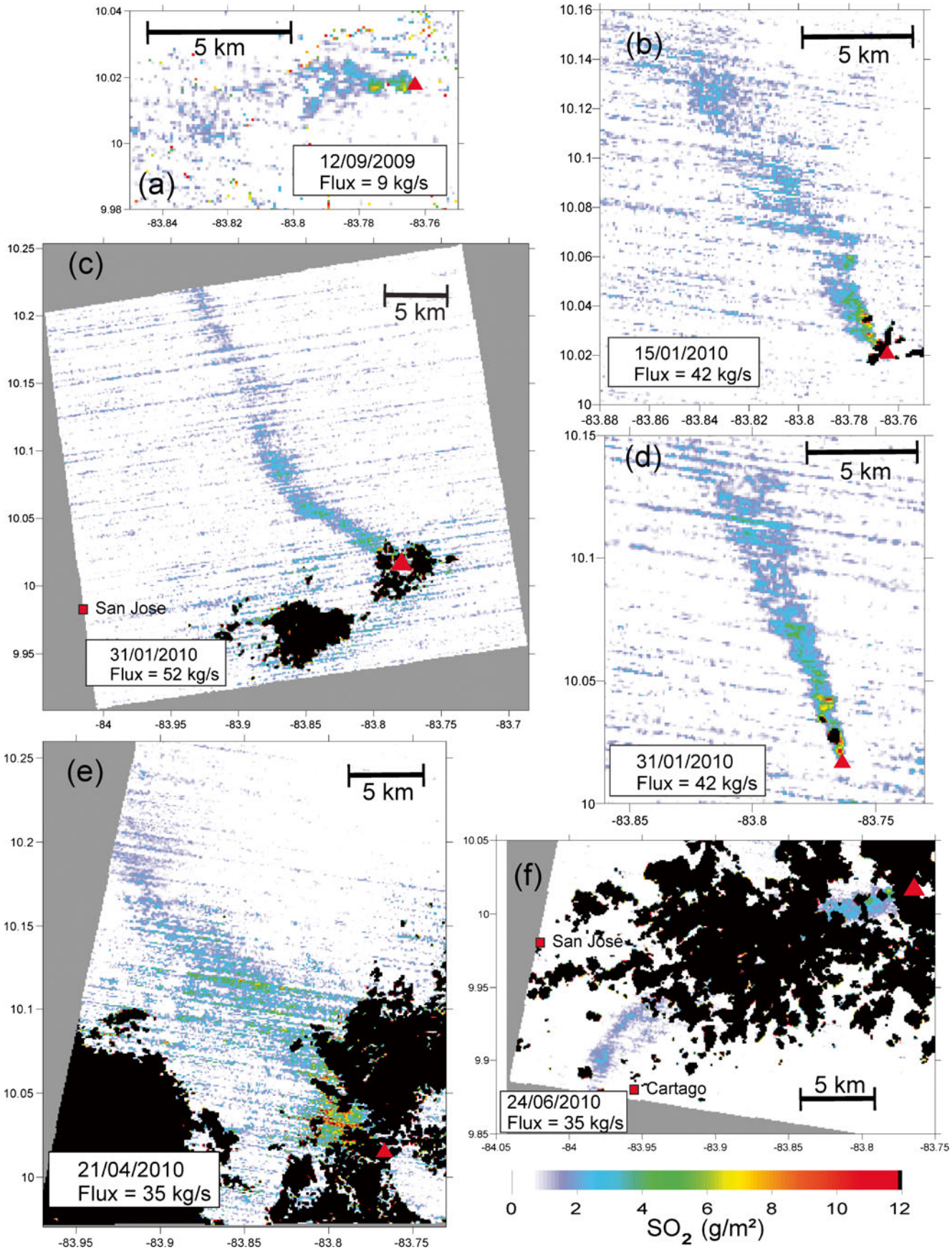
(a)
5 km
12/09/2009
Flux = 9 kg/s
(b)
5 km
15/01/2010
Flux = 42 kg/s
(c)
5 km
San Jose
31/01/2010
Flux = 52 kg/s
(d)
5 km
31/01/2010
Flux = 42 kg/s
(e)
5 km
21/04/2010
Flux = 35 kg/s
(f)
San José
Cartago
5 km
24/06/2010
Flux = 35 kg/s
0 2 4 6 8 10 12
SO2 (g/m²)

◀ **Fig. 3** SO_2 maps of Turrialba plume generated with ASTER images. Colour scale of SO_2 column amounts is the same for all the maps. *Black spots* are pixels where the thermal contrast between the plume and the underlying surface was too low to perform retrievals (clouds or night-cooled highland ground)

five strongest persistent volcanic SO_2 emitters for the year 2010, together with Ambrym, Etna, Nevado de Huila and Tungurahua, (Campion, unpublished data; Nicolas Theys, personal communication, 2011). All these volcanoes show very frequent magmatic activity, with an active lava lake at Ambrym (Smithsonian Institution 2011), rapid lava dome growth at Nevado de Huila (INGEOMINAS website 2010), frequent strombolian eruption at Etna (Smithsonian Institution 2012) or vulcanian explosions at Tungurahua (Instituto Geofisico 2012). By integrating the linear function fitted to the whole dataset between January 2010 and January 2011, we calculated that a cumulative amount of about 1±0.3 Tg of SO_2 has been emitted for the considered period. These high SO_2 flux values constitute a piece of evidence that fresh, gas-rich magma has recently intruded under the volcano. Considering a magma density of 2.5 kg/m^3, an initial S content of 2,500 ppm (value measured in melt inclusions trapped in the olivines of the neighbouring Irazú volcano; Benjamin et al. 2007), and an initial crystal content of 10 %, this would imply the complete degassing of about 75 (±25)×10^6 m^3 of primitive magma. This is more than twice as much as the tephra volume emitted during the last eruptive period of 1864–1866 (<30×10^6 m^3; Reagan et al. 2006), but still categorises it as a small-scale intrusion. The chronology summarised by Martini et al. (2010) suggests that this intrusion was emplaced slowly between 1998 and 2010. Volatiles and heat released by the intrusion interacted with the extensive hydrothermal system of the volcano, creating an expanding hot, vapour-dominated zone around the magmatic intrusion. The percolation of hot gases towards the surface gradually created narrow vapour-dominated pathways, along which the interaction with the colder, liquid-dominated hydrothermal system was reduced, although not suppressed (Fig. 7a). This resulted in the gradual heating and acidification of the summit fumaroles reported by Vaselli et al. (2010), while the chloride enrichment of the fumaroles may have been caused by the high temperature boiling of the acidifying hydrothermal system (Symonds et al. 2001).

A significant increase in fluxes is noted after early January 2010 (Fig. 2). From close to ASTER and OMI detection limit (5–10 kg/s for Turrialba), fluxes increase more than

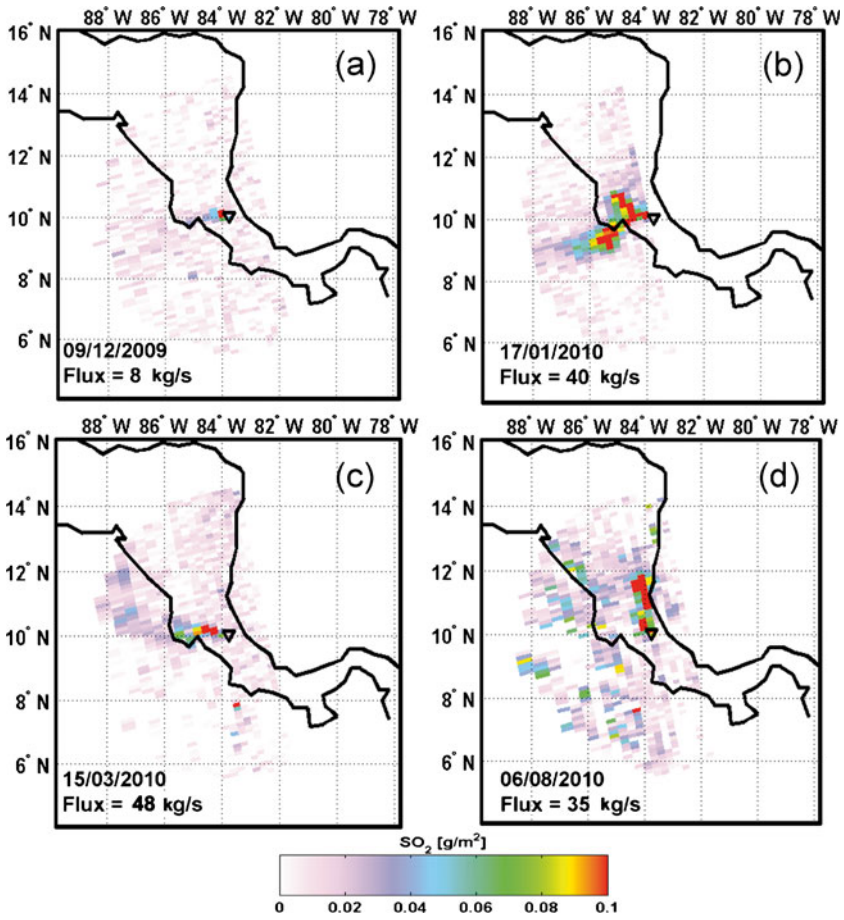

Fig. 4 SO_2 maps of Turrialba plume generated using OMI data. Colour scale of SO_2 column amounts is in g/m^2 and is the same for all the maps

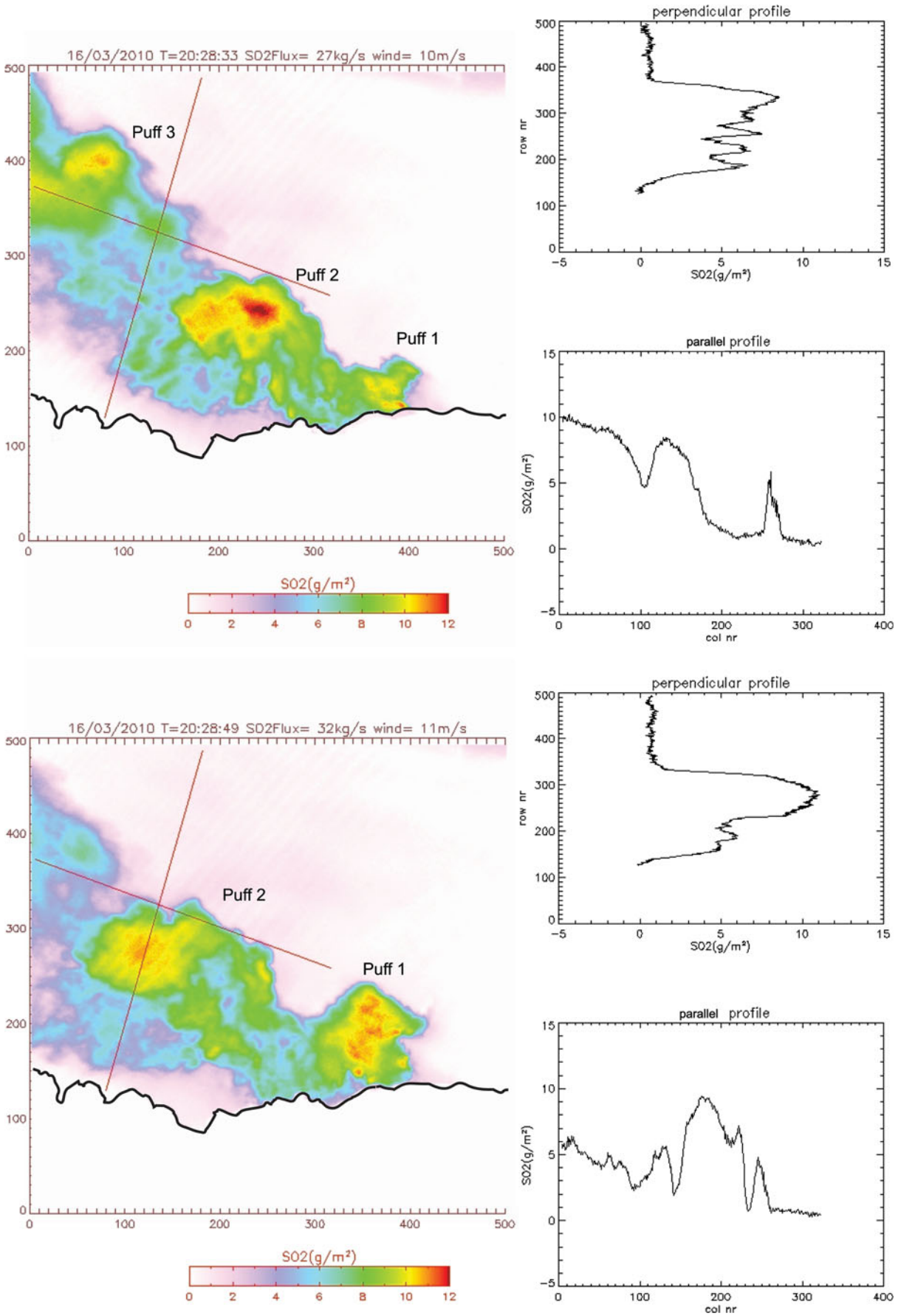
16/03/2010 T=20:28:33 SO2Flux= 27kg/s wind= 10m/s
Puff 3
Puff 2
Puff 1
SO2(g/m²)
perpendicular profile
row nr
SO2(g/m²)
parallel profile
SO2(g/m²)
col nr
16/03/2010 T=20:28:49 SO2Flux= 32kg/s wind= 11m/s
Puff 2
Puff 1
SO2(g/m²)
perpendicular profile
row nr
SO2(g/m²)
parallel profile
SO2(g/m²)
col nr

◀ **Fig. 5** SO_2 measurements obtained with the UV camera. The two images are separated by 16 s. The *left frame of each image* is a map of the column amounts of the plume, the *two right frames* are the SO_2 profiles measured over profiles perpendicular and parallel to the plume transport axis

fourfold, reaching 30–50 kg/s. This increase coincides with a phreatic eruption on 5 January 2010, which opened a new degassing vent in the W crater. Enhanced SO_2 concentrations after this eruption were also detected by in situ measurements using an airborne mass spectrometer (Diaz et al. 2010). This vent was (and is still, in March 2012) persistently emitting high pressure and high temperature gases, producing a jet-like noise and incandescence of the vent inner walls while in the meantime, the vigour and temperature of the other fumarolic fields decreased after the opening of the vent. The most likely explanation of these observations is that after the 5 January explosion (Fig. 7b), most of the gas released by the magma was focused through the new vent, and therefore bypassed the hydrothermal system. We can model the fumarolic activity as the flow of gas through a porous media due to a pressure gradient between the atmosphere and the magma chamber.

We can apply Darcy's law to describe mathematically that model (Turcotte and Schubert 1982), to which we add a loss term to describe the gas scrubbing by the hydrothermal system (Symonds et al. 2001)

$$Q = \frac{kA}{\mu}\frac{(P_m - P_a)}{l} - \varepsilon l \quad (3)$$

where k is the permeability of the rock cap above the magmatic intrusion, k, A and l are the permeability, cross-section and length of the permeable zone above the magma intrusion, respectively, μ is the viscosity of the gas mixture, P_a and P_m are the pressures of the atmosphere and of the magma chamber, respectively, and ε is the scrubbing efficiency. The excavation of the 5th January vent provided a pathway for the gases to flow freely towards the surface, bypassing a significant part of the "porous flow zone". Therefore, as shown in Fig. 7, the parameter l in Eq. 3 was reduced after the eruption and as a result of this Q increased.

It is also possible that the opening of the 5 January vent promoted the degassing of the intruding magma by locally decreasing its confining pressure due to the removal of lithostatic weight. The magnitude of the decompression is difficult to evaluate, since the depth of the 5 January vent is unknown.

The negative slope of the regression lines suggest that SO_2 fluxes have been undergoing a slow decrease since their dramatic increase in early January 2010. This could be the result of a gradual volatile exhaustion of the magma body. If the passive degassing of this recently intruded magma body was to continue, it could lead to its complete gas exhaustion without significant eruption. However, the distance remaining between the magma and the surface is short and occupied by porous, fractured, rocks with consequently weaker mechanical properties (e.g. Montalto 1994). Therefore, an influx of new magma could trigger an eruption with only a short and weak precursory seismic crisis.

The alternative model of this crisis is the passive release of a pre-accumulated S-rich magmatic vapor, slowly accumulated in the unerupted 1864–1866 magma, either (1) because of crystallisation and secondary boiling or (2) because of fluxing (and possibly revitalisation) of the old magma by more deeply rising gas bubbles. We believe that this model is less likely because it does not readily explain the magnitude and duration of the degassing crisis.

A last remarkable aspect of the degassing at Turrialba Volcano since January is that such huge gas fluxes are emitted through a rather narrow vent (~50×20 m, Fernandez et al. 2010a). Experience with high temperature and high flux

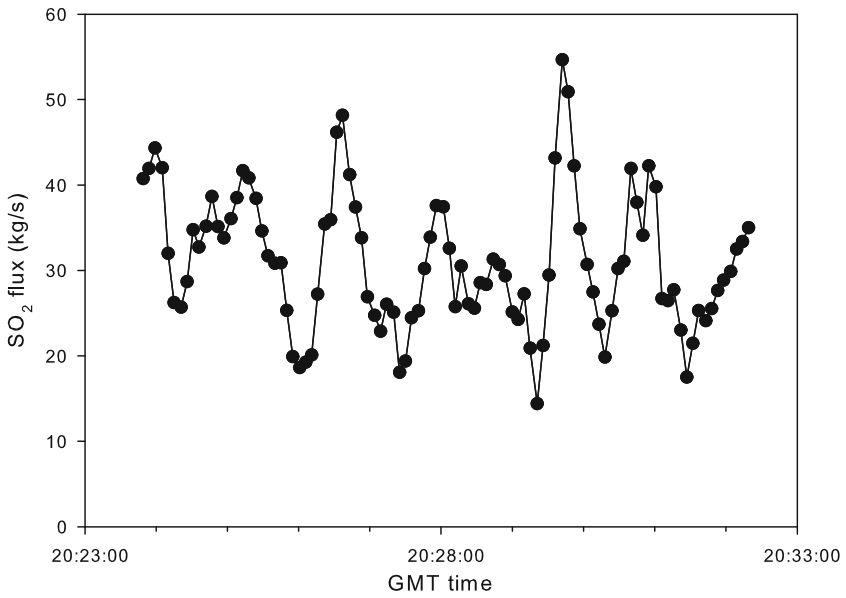

Fig. 6 Ten-minute evolution of the SO_2 flux measured with the UV camera on 15 March 2010. Each peak in the flux was associated to the passage of a puff across the profile traced over the field of view of the camera

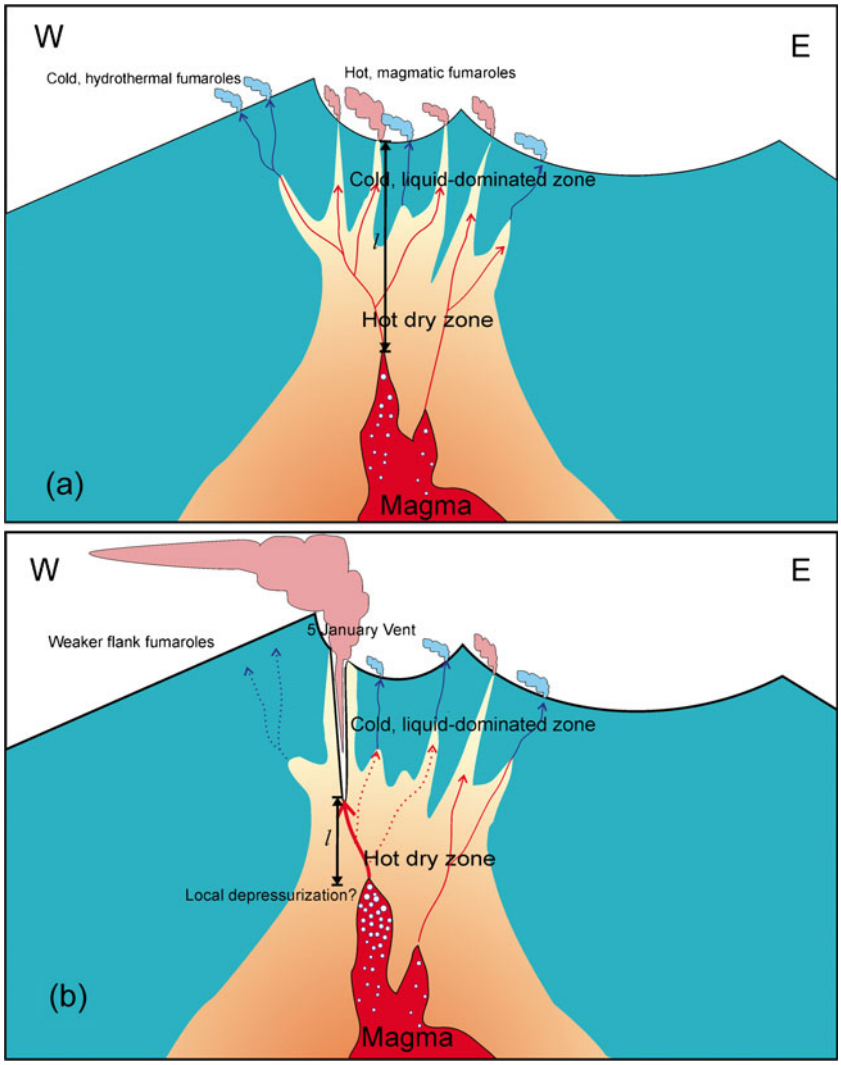

Fig. 7 Hypothetical W–E cross-sections of Turrialba volcano. **a** At the end of 2009. A recently intruded degassing magma body is supplying gases that migrate upwards through narrow hot, dry, vapour-dominated percolation zones. These hot pathways (outlined as *red arrows*) lead to hot fumaroles characterised by a "magmatic" composition, which are concentrated around the W crater. Gases rising through the liquid-dominated hydrothermal system undergo cooling and scrubbing before reaching the surface as cold "hydrothermal" fumaroles. Parameter *l* is the length of the permeable flow pathway (see text). **b** After 5 January 2010. The vent opened by the phreatic explosion concentrates most of the gases emitted by the magma, allowing them to bypass the percolation/scrubbing zone. Therefore, the other fumarolic zones become less alimented and less active. *l* is now significantly reduced. Enhanced degassing is also noted at the top of the magma intrusion, due to the decompression induced by the excavation of the new vent

magmatic degassing through narrow vents tells that these vents are prone to sudden collapses and small-scale explosions. Examples include Kilauea (USGS-HVO 2008a, b), Etna in 1968 and 2010 (Le Guern et al. 1982; Corsaro 2010) and Masaya (Duffel et al. 2003). As these events occur with little warning, the exclusion area around the summit craters should be maintained until the situation stabilises.

Conclusion

SO_2 measurements obtained with three different instruments agree well with each other and have allowed definition of a clear trend in the SO_2 emissions of Turrialba. High SO_2 emissions since January 2010 provide evidence that the decade long unrest at the volcano has been caused by small intrusion of magma, which may have occurred between 2000 and 2010. The volcano has probably entered a new stage, characterised by nearly open-vent magmatic degassing that bypasses the hydrothermal system. The apparent gradual decrease in flux after the January 5 eruption could indicate that the degassing magma body is becoming slowly depleted in volatiles (about 1 Tg of SO_2 has been emitted over the study period). Partial degassing of a rising magmatic intrusion was recognised by Moran et al. (2011) as decreasing the magma buoyancy and promoting the stalling of the intrusion at depth. Even if the gradual degassing of the intruded magma body decreases the probability of an explosive eruption, this study also underlines two hazards associated to the current activity of Turrialba volcano. The first comes from the short distance remaining between the magma chamber and the surface, so that any new magma input could trigger an eruption with only a short precursory seismic crisis. The second results from the narrowness of the degassing vent, which could undergo sudden collapses and/or small-scale explosions. Finally, we think that integrated space-and ground-based imaging techniques probably represent the future of SO_2 measurements at active volcanoes thanks to their good agreement, complementarity, reliability and ease of visualising the measured object at safe distance.

Acknowledgements We thank Dave Pieri for programming ASTER acquisitions of Turrialba during the reported period. R.C. was supported by a grant from FRIA (Fond pour la Recherche Industrielle et Appliquée) and by the VOCATIO foundation, and would like to thank Pierre Quiqueré and Benjamin Morin for their support in the field. Alessandro Aiuppa and two anonymous referees are thanked for their constructive and thorough review and suggestions.

References

Benjamin ER, Plank T, Wade JA, Kelley KA, Hauri EH, Alvarado GE (2007) High water contents in basaltic magmas from Irazú Volcano, Costa Rica. J Volcanol Geotherm Res 168(1-4):68–92

Bobrowski N, Hönninger G, Lohberger F, Platt U (2006) IDOAS: A new monitoring technique to study the 2D distribution of volcanic gas emissions. J Volcanol Geotherm Res 150:329–338

Boichu M, Villament B, Boudon G (2008) A model for episodic degassing of an andesitic magma intrusion. J Geophys Res 113: B07202. doi:10.1029/2007JB005130

Campion R, Salerno GG, Coheur P, Hurtmans D, Clarisse L, Kazahaya K, Burton M, Caltabiano T, Clerbaux C, Bernard A (2010) Measuring volcanic degassing of SO2 in the lower troposphere with ASTER band ratios. J Volcanol Geotherm Res 194(1–3):42–54

Capasso G, Favara R, Francofonte S, Inguaggiato S (1999) Chemical and isotopic variations in fumarolic discharge and thermal waters at Vulcano Island (Aeolian Islands, Italy) during 1996: evidence of resumed volcanic activity. J Volcanol Geotherm Res 88:167–175

Carn SA, Krueger AJ, Arellano S, Krotkov NA, Yang K (2008) Daily Monitoring of Ecuadorian volcanic degassing from space. J Volcanol Geotherm Res 176:141–150

Carr MJ, Feigenson MD, Patino LC, Walker JA (2003) Volcanism and geochemistry in Central America: progress and problems. AGU Geophysical Monograph 138:153–174

Cheminée J-M, Javoy M, Delorme H (1983) Temperature and gas data from Turrialba, SEAN 08.01, Smithsonian Institution, http://www.volcano.si.edu/world/volcano.cfm?vnum=1405-07=&volpage=var#sean_0801

Corsaro RA (2010) INGV weekly volcanological report on Etna activity, 5–11 March 2010, http://www.ct.ingv.it/index.php?option=com_docman&task=doc_download&gid=1662&Itemid=330. Accessed December 2010)

Dalton MP, Watson IM, Nadeau P, Werner C, Morrow W, Shannon JM (2009) Assessment of the UV camera sulphur dioxide retrieval for point source plumes. J Volcanol Geoth Res 188:358–366

Diaz JA, Pieri D, Arkin CR, Gore E, Griffin TP, Fladeland M, Bland G, Soto C, Madrigal Y, Castillo D, Rojas E, Achi S (2010) Utilization of in situ airborne MS-based instrumentation for the study of gaseous emissions at active volcanoes. Internat J Mass Spectrometry 295-3:105–112

Duffell HJ, Oppenheimer C, Pyle DM, Galle B, McGonigle AJS, Burton MR (2003) Changes in gas composition prior to a minor explosive eruption at Masaya volcano, Nicaragua. J Volcanol Geotherm Res 126:327–339

Fernández E, Duarte E, Sáenz W, Marino T, Martínez M, Brenes J, OVSICORI-UNA (2010a) Estado de los volcanes Enero del 2010. http://www.ovsicori.una.ac.cr/index.php?option=com_phocadownload&view=category&download=118:estado-volcanes-enero-2010&id=18:2010&Itemid=73. Accessed May 2012

Fernández E, Martínez M, Sáenz W, Villegas M, Duarte E, OVSICORI-UNA, (2010b) Estado de los volcanes abril del 2010. http://www.ovsicori.una.ac.cr/index.php?option=com_phocadownload&view=category&download=122:estado-volcanes-abril-2010&id=18:2010&Itemid=73. Accessed May 2012.

Fernández E, Martínez M, Sáenz W, Duarte E, Brenes J, Villalobos A, OVSICORI-UNA, (2010c) Estado de los volcanes agosto del 2010. www.ovsicori.una.ac.cr/index.php?option=com_phocadownload&view=category&download=125:estado-volcanes-agosto-2010&id=18:2010&Itemid=73. Accessed May 2012

Fischer TP, Arehart GB, Sturchio NC, Williams SN (1996) The relationship between fumarole gas composition and eruptive activity at Galeras Volcano (Colombia). Geology 24:531–534

Galle B, Johansson M, Rivera C, Zhang Y, Kihlman M, Kern C, Lehmann T, Platt U, Arellano S, Hidalgo S (2009) NOVAC—a global network for volcano gas monitoring: network layout and instrument description. J Geophys Res Atmos 115:D05304

INGEOMINAS (2010) Monthly bulletins of activity for Nevado del Huila volcano in 2010 http://intranet.ingeominas.gov.co/popayan/Comunicados_2010#Boletines_mensuales_de_actividad. Accessed May 2012

Instituto Geofisico (2012) Actividad del Volcán Tungurahua - Diciembre 2010 http://www.igepn.edu.ec/images/collector/collection/informes-volcanicos/tungurahua/resmentungdic10.fin.pdf (accessed May 2012)

Kantzas EP, McGonigle AJS, Tamburello G, Aiuppa A, Bryant RG (2010) Protocols for UV camera volcanic SO_2 measurements. J Volcanol Geotherm Res 194:55–60

Kern C, Deutschmann T, Vogel L, Wöhrbach M, Wagner T, Platt U (2010a) Radiative transfer corrections for accurate spectroscopic measurements of volcanic gas emissions. Bull Volc 72:233–247. doi:10.1007/s00445-009-0313-7

Kern C, Kick F, Lübcke P, Vogel L, Wöhrbach M, Platt U (2010b) Theoretical description of functionality, applications, and limitations of SO2 cameras for the remote sensing of volcanic plumes. Atmos Meas Tech 3:733–749

Kinoshita K (1996) Observation of flow and dispersion of volcanic clouds from Mt. Sakurajima. Atmos Environ 30(16):2831–2837

Krotkov NA, Carn SA, Krueger AJ, Bhartia PK, Yang K (2006) Band residual difference algorithm for retrieval of SO_2 from the Aura Ozone Monitoring Instrument (OMI). IEEE Trans Geosc Rem Sens 44(5):1259–1266

Le Guern F, Tazieff H, Vavasseur C, Zettwoog P (1982) Resonance in the gas discharge of the Bocca Nuova, Etna (Italy), 1968-1969. J Volcanol Geotherm Res 12:161–166

Levelt PF, van den Oord GHJ, Dobber MR, Mälkki A, Visser H, de Vries J, Stammes P, Lundell J, Saari H (2006) The Ozone Monitoring Instrument. IEEE Trans Geosci Remote Sens 44 (5):1093–1101

Martini F, del Potro R, Martínez M, van der Laat R, Tassi F, Vaselli O (2010) Geophysical, geochemical and geodetical signals of reawakening at Turrialba volcano (Costa Rica) after almost 150 years of quiescence. J Volcanol Geotherm Res 198:416–432. doi:10.1016/j.jvolgeores.2010.09.021

Montalto A (1994) Seismic signals in geothermal areas of active volcanism: a case study from "La Fossa", Vulcano (Italy). Bull Volcanol 56:220–227

Moran SC, Newhall C, Roman DC (2011) Failed magmatic eruptions: Late-stage cessation of magma ascent. In: Moran SC, Newhall CG, Roman DC (eds) Failed eruptions: Late-stage cessation of magma ascent. Bull Volcanol 73(2):115–122

Mori T, Burton MR (2006) The SO_2 camera: a simple, fast and cheap method for groundbased imaging of SO_2 in volcanic plumes. Geophys Res Lett 33:L24804

Mori T, Mori T, Kazahaya K, Ohwada M, Hirabayashi J, Yoshikawa S (2006) Effect of UV scattering on SO_2 emission rate measurements. Geophys Res Lett 33:L17315

Oppenheimer C, Scaillet B, Martin RS (2011) Sulfur degassing from volcanoes. Source Cond Surveill Plume Chem Rev Mineral Geochem 73:363–421

Pieri D, Abrams M (2004) ASTER watches the world's volcanoes: a new paradigm for volcanological observations from orbit. J Volcanol Geotherm Res 135:13–28

Reagan M, Duarte E, Soto GJ, Fernández E (2006) The eruptive history of Turrialba volcano, Costa Rica, and potential hazards from future eruptions. In: Rose W I, Bluth GJS, Carr MJ, Ewert JW, Patino LC, Vallance JW (eds), Volcanic hazards in Central America, Geol Soc Amer Spec Pap 412: 235–257

Smithsonian Institution (2011) Ambrym, Bull. Global Volcanism Network, 36:05

Smithsonian Institution (2012) Etna, Bull. Global Volcanism Network, 37:02

Stoiber RE, Maliconico LL, Williams SN (1983) Use of the correlation spectrometer at volcanoes. In: Tazieff H, Sabroux J-C (eds) Forecasting volcanic events. Elsevier, Amsterdam, pp 425–444

Symonds RB, Gerlach TM, Reed MH (2001) Magmatic gas scrubbing: implications for volcano monitoring. J Volcanol Geotherm Res 108:303–341

Tamburello G, Kantzas EP, McGonigle AJS, Aiuppa A, Giudice G (2011) UV camera measurements of fumarole field degassing (La Fossa crater, Vulcano Island). J Volcanol Geotherm Res 199:47–52

Thomas HE, Watson IM (2010) Observations of volcanic emissions from space: current and future perspectives. Nat Hazards 54:323–354. doi:10.1007/s11069-009-9471-3

Turcotte DL, Schubert G (1982) Geodynamics: applications of continuum physics to geological problems. Wiley, New York, pp 381–422

USGS-HVO, United States Geological Survey Hawaii Volcano Observatory, News Release, March 14 2008, New gas vent in Halema'uma'u crater doubles sulfur dioxide emission rates. http://hvo.wr.usgs.gov/pressreleases/pr03_14_08.html. Accessed Jan 2010

USGS-HVO, United States Geological Survey Hawaii Volcano Observatory, News Release, March 19, 2008, Explosive eruption in Halema`uma`u Crater, Kilauea Volcano, is first since 1924 http://hvo.wr.usgs.gov/pressreleases/pr03_19_08.html. Accessed Jan 2010

Vaselli O, Tassi F, Duarte E, Fernández E, Poreda R, Huertas J (2010) Evolution of fluid geochemistry at the Turrialba volcano (Costa Rica) from 1998 to 2008. Bull Volcan 72(4):397–410

Yang K, Krotkov NA, Krueger AJ, Carn SA, Bhartia PK, Levelt PF (2007) Retrieval of large volcanic SO_2 columns from the Aura Ozone Monitoring Instrument: Comparison and limitations. J Geophys Res 112:D24S43

Zlotnicki J, Boudon G, Le Mouel J-L (1992) The volcanic activity of La Soufrière de Guadeloupe (Lesser Antilles): structural and tectonic implications. J Volcanol Geotherm Res 49:91–104